Tellus (1981), *33*, 274–290

A comparison of several models of carbon turnover in the ocean with respect to their distributions of transit time and age, and responses to atmospheric CO_2 and ^{14}C

By GEORGE G. KILLOUGH, *Health and Safety Research Division*[1]
and WILLIAM R. EMANUEL, *Environmental Sciences Division*,
Oak Ridge National Laboratory, Oak Ridge, Tennessee 37830, U.S.A.

(Manuscript received May 20; in final form September 4, 1980)

ABSTRACT

Five models of carbon depth distribution in the world ocean are compared with respect to carbon transit-time distribution, age distribution, and integrated responses to histories of fossil CO_2 and weapons ^{14}C. Two models represent the ocean as two well-mixed layers and differ only in the relative sizes of these compartments. The remaining three models consider 19 well-mixed layers and differ in the patterns of carbon transfer among the layers. All five models are required to be compatible with a preindustrial depth profile of natural ^{14}C, which is used to fix the values of transfer coefficients. Within this constraint the five models exhibit significantly different responses to fossil CO_2 and weapons ^{14}C regimes. Of the estimated 134×10^{15} g of fossil carbon produced in the period 1860–1975, the models estimate a net uptake range of 24×10^{15} to 66×10^{15} gC by the ocean. For weapons ^{14}C the range is 6.0×10^{2} to 1.0×10^{3} kg ^{14}C. Each of these models shows shifts in the implied role of the terrestrial biota between net carbon source and sink, with the latter role dominating in the last years of the simulated period. The largest estimate of source strength for the five models was 0.74×10^{15} gC yr^{-1}, in contrast to the fossil CO_2 production rate of $\sim 5 \times 10^{15}$ gC yr^{-1} in 1975. The five models were also used to predict atmospheric CO_2 levels during the period 1975–2300 for a logistic source that would ultimately release 5000×10^{15} gC.

1. Introduction

Attempts to predict future atmospheric increases of carbon dioxide that could result from fossil fuel combustion depend on mathematical models of the global carbon cycle. Such models generally divide the cycle into reservoirs representing carbon in the atmosphere, terrestrial biota, and the oceans. These reservoirs are often further subdivided into well-mixed boxes or compartments representing either subsystems (e.g., photosynthesizing parts of plants, woody tissue, litter, humus, and decomposers) or discrete strata of spatial distribution (such as layers of ocean water or geographical location of ecosystem types). The mathematical formulation of such a dynamic model of the carbon cycle takes the form of a system of operator equations (usually differential) which relate transfers of carbon among compartments to the dynamic levels within the compartments. Reviews of global carbon cycle modeling have been given by Bolin (1975) and Keeling (1973a).

In previous modeling efforts, the radioactive carbon isotope ^{14}C has been used as a tracer for total carbon cycling (Craig, 1957; Revelle and Suess, 1957). Measurements of ^{14}C activity in various reservoirs both before and after the large input of ^{14}C due to above-ground testing of nuclear weapons since the 1940s, and particularly in the early 1960s, have been used in calibration and testing of global carbon cycle models. Recent dynamic models of carbon circulation in the world oceans have exploited ^{14}C depth distribution data

[1] Publication No. 1601, Environmental Sciences Division, Oak Ridge National Library.

0040-2826/81/030274-17$02.50/0

for calibration (e.g., Broecker et al., 1960; Keeling, 1973a; Bacastow and Keeling, 1973; Oeschger et al., 1975; Siegenthaler and Oeschger, 1978; Björkström, 1979; Killough, 1980).

A box model determines distributions for the transit time of carbon entering the ocean reservoir and for the age of carbon resident in the ocean. These model distributions are potentially helpful in interpreting tracer measurements (e.g., natural or man-made radioactive ^{14}C) from ocean water. The steady-state transit-time distribution is particularly useful as a succinct picture of the intrinsic dynamic characteristics of a model reservoir and provides a basis for comparison with the response of the corresponding reservoir of alternative models. Transit-time and age distributions and their bearing on reservoir dynamics and interpretation of tracers have been discussed in a general setting by Eriksson (1961), Bolin and Rodhe (1973), Nir and Lewis (1975), and Lewis and Nir (1978).

We have formulated five models of carbon circulation in the global ocean which, insofar as their structures permit, are required to be consistent with the same hypothesized depth distribution of radiocarbon activity. The steady-state distributions of transit time and carbon age are determined explicitly for each model. Our calculations show that predictions of the fate of CO_2 released to the atmosphere can vary significantly, despite the common ^{14}C calibration. The models' range of estimates of historic uptake of fossil-fuel CO_2 by the ocean is nearly three times the minimum estimate. Moreover, the calculations suggest that the role of the terrestrial biota in the cycle as source or sink for excess carbon may have shifted from one to the other several times during the period 1860–1975, although the role of sink appears to have become dominant in the years immediately preceding 1975.

2. Structural definitions of models

The five models considered here divide the ocean into a surface layer and a deeper portion, with all carbon that is exchanged with the atmosphere passing through the former compartment. For convenience, the models are designated 1 (a and b), 2 and 3 (a and b).

Model 1 consists of a surface layer and a deep-water reservoir which exchange carbon by linear donor-controlled fluxes. Model 1a (Fig. 1) is based on a surface-layer depth of 75 m (the mean depth of the top of the thermocline; see Craig, 1957), a choice that is consistent with Models 2 and 3. In Model 1b (Fig. 1), the depth of the surface layer is taken to be 260 m, which approximates a value arrived at by Bacastow and Keeling (1979) in a series of calibration exercises with a geochemical model of the carbon cycle that incorporates a similar two-box ocean.

The three remaining models consist of a single 75-meter surface layer and a deep reservoir that is subdivided into 18 horizontal layers (Fig. 2 and Table 1). These layered models differ from each other only in the topological configuration of fluxes among the layers.

Of the layered group, Model 2 injects carbon from the surface layer directly into each of the deep-water layers, and each deep layer returns it directly to the surface layer; there is no direct mixing of carbon among the deep layers. This model might be interpreted as an extreme view that the total downward transport of carbon is by the sinking of cold surface water and its return to the surface is exclusively due to upwelling.

Models 3a and 3b (Fig. 2), also in the layered group, move carbon upward through the deep water reservoir by transfers from layer to layer. Model 3b represents downward transport in the same way, with passage through successive layers, whereas Model 3a uses direct injection from the surface layer to the deep water layers as in Model 2. These downward pathways represent sinking

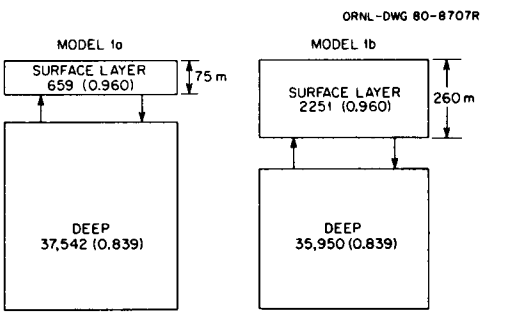

Fig. 1. Two-box Models 1a and 1b. The numbers inside the boxes are their masses of elemental carbon (units of 10^{15} g) and ^{14}C activities (parenthesized; normalized to the atmospheric value) assumed for the preindustrial steady state. These models differ only in the depths of their surface layers.

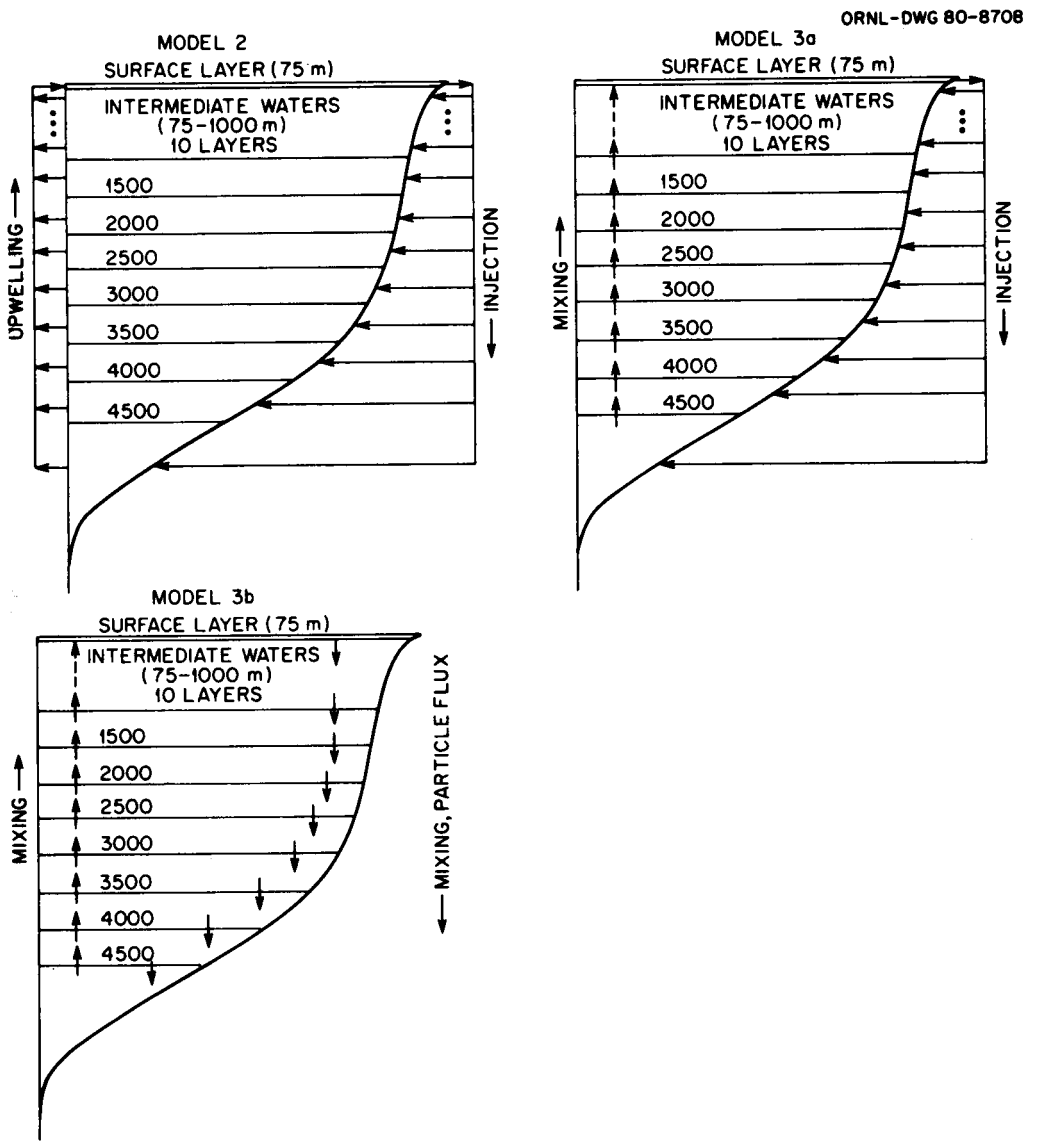

Fig. 2. Layered Models 2, 3a, and 3b. Assignments of carbon and ^{14}C activity to the layers are given in Table 1 and are identical for the three models. Areas of the layers are proportional to the respective water volumes as calculated from Sverdrup et al. (1942). Patterns of carbon flow that distinguish the three models from each other are indicated by the arrows.

polar waters as the transport vehicle in the latter case and turbulent mixing combined with the flux of organic particles in the former.

The two-box models, 1a and 1b, are simpler than those employing multiple layer constructs, making them amenable to analytical solution (e.g., Keeling, 1973a). Keeling and Bacastow (1977) and Bacastow and Keeling (1979) have shown that for careful choice of model parameters (in particular their choice of depth of the surface layer approximates the 260-meter value in our model 1b), the response of the two-box representation (at least with respect to atmospheric CO_2) is in fair agreement with the "box-diffusion" model of Oeschger et al. (1975), in which the ocean can be interpreted as a multiple-layer construct.

Table 1. *Distribution of nonradioactive carbon and natural ^{14}C for the five ocean models*

Layer i	Depth (m)	Nonradioactive carbon y_i^0 (10^{15} g)		^{14}C activity A_i'	
		1a	1b	1a	1b
1	0		659		0.960
2	75		432		0.959
3	125		643	2251	0.957	0.960
4	200		862		0.953
5	300 [260]		880		0.939
6	400		895		0.925
7	500		895		0.914
8	600		895		0.909
9	700		895		0.904
10	800		895		0.900
11	900	37,542	893	0.839	0.896
12	1000		4437	35,950	0.885	0.839
13	1500		4328		0.864
14	2000		4187		0.837
15	2500		4015		0.814
16	3000		3678		0.795
17	3500		3177		0.781
18	4000		2506		0.770
19	4500		3029		0.723

$$M = \Sigma y_i^0 = 38{,}201$$

Model 3b bears some similarity to the "box diffusion" model of Oeschger et al. (1975) and is structurally identical (except in the number of layers) to a model used by Killough (1980) in assessing worldwide population exposure to releases of ^{14}C from nuclear fuel cycles. The "box diffusion" model, however, treats the ocean as a cylinder in which the steady-state concentration of nonradioactive carbon is uniform with depth, whereas the layered models treated in this paper (Models 2, 3a, and 3b) take account of the dependence of the ocean's horizontal cross-sectional area and carbon concentration on depth. The "box diffusion" model also subdivides the deep ocean into a larger number of layers (42) than the models described in this paper.

A model under development by A. Björkström and others (Björkström, 1979; Bolin, 1975) emphasizes carbon transport into the deep ocean by way of sinking cold surface waters in the high latitudes and in this respect resembles Model 3a. However, (1) the Björkström model explicitly divides the surface waters into a warm and a cold compartment, with only the latter supplying carbon directly to the deep layers; (2) the Björkström model incorporates direct feedback from the two layers with which it represents intermediate waters (75 → 1000 m) to the cold surface-water compartment; (3) the biotic particle flux is given explicit treatment by Björkström. Model 3a must be viewed as a simplified prototype which focuses attention on the sinking water transport.

Notwithstanding the different patterns of exchange, the five models are required to be consistent with respect to hypothesized preindustrial distributions of nonradioactive carbon and natural ^{14}C activity among their compartments. Each model's nonzero transfer coefficients (corresponding to the flows shown in its diagram in Figs. 1 or 2) are uniquely determined from its steady-state equations of carbon transfer and the assumed carbon inventories and ^{14}C activities. For each layer, a pair of equations is written for the steady-state: the first expresses the net rate of loss (= zero) of nonradioactive carbon from the compartment and the second that of naturally produced ^{14}C (= rate of radioactive decay) with isotope fractionation eliminated. The transfer rate coefficients obtained as solutions of these equations are therefore compatible with the preindustrial

fractionation-corrected ^{14}C and the total carbon depth distributions shown in Table 1.

Surface waters: layer 1

$$I - \left(\mu + \sum_{j=2}^{N} k_{1,j}\right) y_1^0 + \sum_{j=2}^{N} k_{j,1} y_j^0 = 0 \tag{2.1}$$

$$I - \left(\mu + \sum_{j=2}^{N} k_{1,j}\right) A_1' y_1^0 + \sum_{j=2}^{N} k_{j,1} A_j' y_j^0 = \lambda A_1' y_1^0 \tag{2.2}$$

Deep waters: layer $i = 2, \ldots, N$

(Note: [ ] means the enclosed term is omitted if $i = 2$; { } is omitted if $i = N$.)

$$[k_{1,i} y_1^0] + k_{i-1,i} y_{i-1}^0 - (k_{i,i-1} + \{k_{i,i+1}\} + [k_{i,1}]) y_i^0 + \{k_{i+1,i} y_{i+1}^0\} = 0 \tag{2.3}$$

$$[k_{1,i} A_1' y_1^0] + k_{i-1,i} A_{i-1}' y_{i-1}^0 - (k_{i,i-1} + \{k_{i,i+1}\} + [k_{i,1}]) A_i' y_i^0 + \{k_{i+1,i} A_{i+1}' y_{i+1}^0\} = \lambda A_i' y_i^0 \tag{2.4}$$

For $N = 2$, eqs. (2.1)–(2.4) define the steady state for Models 1a and 1b; for Models 2, 3a, and 3b, $N = 19$. The numbering of the layers ($i = 1, \ldots, N$) increases with depth. The notations used in the foregoing equations are as follows:

I = total carbon invasion rate from the atmosphere in preindustrial steady state (= 97.2 $\times 10^{15}$ g yr^{-1});

μ = total carbon evasion rate coefficient for movement from surface waters to atmosphere (= 0.148 yr^{-1} for Models 1a, 2, 3a, and 3b; 0.0432 yr^{-1} for Model 1b);

$k_{i,j}$ = transfer rate coefficient from compartment i to j (yr^{-1});

y_i^0 = ^{12}C + ^{13}C inventory in compartment i in preindustrial steady state (g; Table 1);

A_i' = preindustrial $^{14}C/^{12}C$ ratio in layer i, corrected for isotope fractionation and normalized to the atmospheric value (dimensionless; Table 1);

λ = radioactive decay rate coefficient for ^{14}C (= 1.21 $\times$ 10^{-4} yr^{-1}, based on a half-life of 5730 yr).

When those $k_{i,j}$ that do not appear in the model under consideration are set equal to zero, eqs. (2.3) and (2.4) determine a linear algebraic system of rank $2(N - 1)$, which may be solved for the model's nonzero $k_{i,j}$. From eqs. (2.1)–(2.4) one may derive

$$I = \mu y_1^0 = \frac{\lambda \sum_{j=1}^{N} A_j' y_j^0}{1 - A_1'} \tag{2.5}$$

from which one verifies, with the aid of Table 1, that the steady-state invasion rate I is the same for all five models.

We summarize here some of the limitations of the five models, expressed in terms of processes or features not taken into explicit consideration:

downward flux of particulate biotic material;

dissolution of mineral carbonates as the uptake of CO_2 lowers the pH of ocean water (Keeling and Bacastow, 1977);

spatial disaggregation that would permit consideration of nonuniformly distributed properties (e.g., warm vs cold surface waters; separation of Atlantic and Pacific Oceans);

calibration or validation with distributed tracers other than radiocarbon (e.g., ^{13}C—Stuiver, 1978; oxygen profiles—Björkström, 1979; Kuo and Veronis, 1973; other isotopes—^{3}H, ^{90}Sr, ^{222}Rn, ^{226}Ra— Broecker, 1963; Broecker et al., 1979);

exchange of carbon with marine sediments;

river input of carbon;

clear distinction between dissolved organic and inorganic carbon, with the former constituting about 4% of dissolved carbon in the ocean (Keeling, 1973a).

3. Mass distribution of natural ^{14}C activity in the ocean

Data on which our model calibrations are based are expressed in terms of the quantity $\Delta\,^{14}C$. The value of $\Delta\,^{14}C$ for a carbon sample is interpreted as the per-mil (‰) depletion of the $^{14}C/^{12}C$ ratio of the sample from that of average 19th century wood (corrected for ^{14}C decay from the time of fixation to January 1, 1958) with the effect of isotope fractionation being removed by comparison with the sample's $^{13}C/^{12}C$ ratio (Broecker and Olson, 1959). Thus $\Delta\,^{14}C = 0$ for a typical sample of 19th century wood and for CO_2 in the 19th century atmosphere.

The quantity A' introduced in section 2 is related to $\Delta\,^{14}C$ as follows:

$$A' = 1 + \frac{\Delta\,^{14}C}{1000} \tag{3.1}$$

so that $A' = 1$ for the preindustrial atmosphere. For natural radiocarbon in the ocean, we seek to estimate the cumulative distribution of A' with respect to carbon mass:

$M \cdot F(A')$ = mass of carbon in the ocean for which ^{14}C activity is less than A' (3.2)

where M denotes the total mass of carbon in ocean water and $F(A')$ is the normalized cumulative distribution function. Direct sampling to establish this distribution could have been accomplished in the 19th century but is no longer possible because of the dilution of natural ^{14}C activity by the fossil carbon dioxide taken up by the ocean and, more importantly, because of the ocean's uptake of significant quantities of excess ^{14}C produced by detonations of nuclear weapons since the 1940s. For calibration of the five models, we have used the procedure described below to estimate the distribution (3.2) of A'.

Our first concern was to select data to minimize the contamination by penetration of the weapons-produced ^{14}C. Bien and Suess (1967) extrapolated from samples of comparable depth profiles of ^{14}C activity over time and concluded that as of the mid-1960s weapons ^{14}C had not penetrated significantly below 200 m in the waters of the Pacific. For our calibration we extended this hypothesis to all oceans and selected only those samples taken at depths equal to or greater than 200 m reported by Bien et al. (1965) for the Pacific and Indian Oceans, and by Broecker et al. (1960) for the Atlantic. More recent data have been deliberately excluded in view of evidence of deeper incursion of the weapons ^{14}C (Stuiver and Östlund, 1980; Östlund and Stuiver, 1980). Our data base for the waters below 200 m consists of 191 sample points: 81 from the Atlantic, 62 from the Pacific, and 48 from the Indian Ocean.

To obtain a carbon mass distribution of $\Delta\,^{14}C$ (and hence A') in the ocean, we must determine suitable weights for the sample $\Delta\,^{14}C_n$ values. We assume the entire sampling plan to have been stratified, such that each $\Delta\,^{14}C_n$ is representative of the carbon mass in the stratum from which it is drawn. The strata are taken as horizontal layers of water, six each in the Pacific and Indian Oceans and seven in the Atlantic. As defined by arbitrary depth intervals, the strata are given in Table 2. The weight or "frequency," f_n, of sample point $\Delta\,^{14}C_n$ is

$$f_n = \frac{1}{N_{S(n)}} \cdot \frac{M_{S(n)}}{M_{200}} \tag{3.3}$$

where $S(n)$ denotes the stratum from which the nth sample point was drawn, $N_{S(n)}$ the number of sample points taken in $S(n)$, $M_{S(n)}$ the mass of carbon in $S(n)$, and M_{200} the total carbon mass in the ocean below the 200-meter depth. Summed over the 191 sample points, these weights add to unity. Estimates of the fractions $M_{S(n)}/M_{200}$ (Table 2) are based on hypsographic data (Sverdrup et al., 1942) and on concentration profiles for dissolved inorganic carbon (e.g. Broecker, 1974). The estimate of surface concentration, 2.056 mol m^{-3}, is based on equilibration of dissolved CO_2 with assumed preindustrial atmospheric partial pressure of 290 ppm by volume at temperature 292.75 K (Keeling, 1973a).

The empirical cumulative distribution function $\hat{F}_{200}(A')$ for carbon in the ocean below 200 m may now be defined:

$$\hat{F}_{200}(A') = \sum_{\{n:A'_n < A'\}} f_n \tag{3.4}$$

where A' is related to $\Delta\,^{14}C$ by eq. (3.1). The notation in braces indicates that the sum is to be taken over those n for which the condition $A'_n < A'$ is satisfied. For those A' less than all A'_n, the sum is defined as zero.

Table 2. *Estimated fractional distribution of carbon in the deep oceans, stratified by depth intervals*

Depth interval (m)	Atlantic	Pacific	Indian
200–500	0.019 (11)*	0.037 (6)	0.016 (9)
500–1000	0.031 (12)	0.064 (8)	0.027 (3)
1000–2000	0.060 (18)	0.127 (12)	0.054 (9)
2000–3000	0.054 (14)	0.120 (15)	0.051 (7)
3000–4000	0.044 (4)	0.103 (19)	0.041 (14)
4000–5000	0.027 (6)	0.087 (2)	0.029 (6)
≥5000	0.009 (16)		
Totals	0.244 (81)	0.538 (62)	0.218 (48)

* Numbers in parentheses give the numbers of $\Delta\,^{14}C$ sample points in the respective strata.

Fig. 3 shows the empirical distribution (3.4) of A'. Superimposed on this graph is a coarser step function that adapts the distribution to the resolution permitted by the 16 layers of Models 2, 3a, and 3b that correspond to depths of 200 m and below.

Table 1 extends the distribution of A' to the upper 200 m of the ocean, which in the layered models consists of the surface layer (0 → 75 m) and two intermediate layers (75 → 125 and 125 → 200 m). We assign $A' = 0.96$ to the surface layer (Keeling, 1973a; Broecker et al., 1978) and use linear interpolation to complete the assignment for the two intervening layers. The allocations of A' and carbon mass between the layers of the two-box models (1a and 1b) are also indicated in Table 1.

Our estimate of the distribution of A', to the resolution of our layered models, may be given as

$$\hat{F}(A') = \sum_{\{i:A_i' < A'\}} y_i^0/M \tag{3.5}$$

where y_i^0/M is the estimated fraction of the ocean's carbon mass in layer i, with y_i^0 and M as given in Table 1. The notation A_i' in eq. (3.5) means the activity assigned to layer i, in contrast to a similar notation with subscript n used earlier to denote sample values.

For the vertical-transport models under consideration, eq. (3.5) establishes an effective depth profile of natural ^{14}C activity. Fig. 4 shows our effective profile superimposed on tracings of observed profiles in the Pacific and Indian Oceans by Bien et al. (1965) and ranges of activity in various depth zones in the Atlantic from the data of Broecker et al. (1960).

The foregoing method for assigning ^{14}C activities to the layers of Models 2, 3a, and 3b enforces two requirements: (1) activity must decrease monotonically with increasing depth, and (2) the carbon-mass distribution of

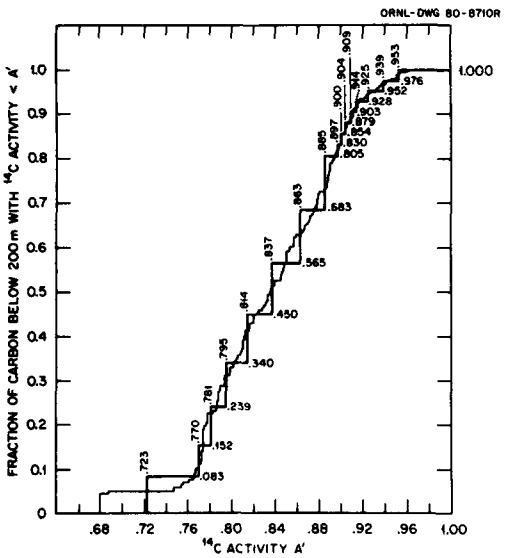

Fig. 3. Cumulative distribution of ^{14}C activity in the ocean below 200 m. This region is assumed to be typical of pre-bomb steady state, and ^{14}C activity A' is normalized to the preindustrial atmospheric value. The empirical distribution curve is based on 191 observations of $\Delta\,^{14}C$ reported by Broecker et al. (1960) for the Atlantic and Bien et al. (1965) for the Pacific and Indian Oceans. The coarser graph is an adaptation to the resolution permitted by the 19-layered Models 2, 3a, and 3b. The horizontal numbers are cumulative fractions of carbon mass below 200 m that correspond to cumulation of these layers' carbon content from the bottom upward (A' decreases with increasing depth).

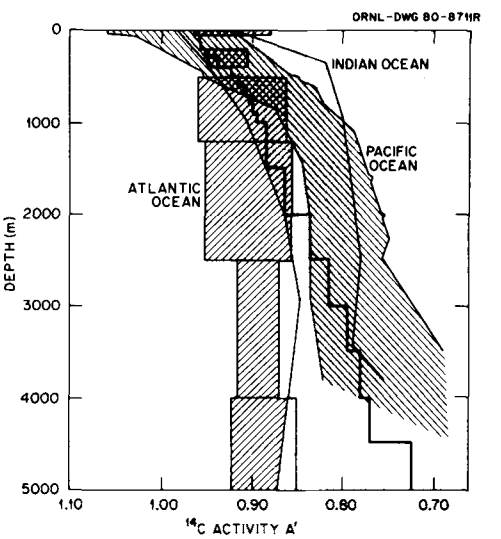

Fig. 4. Calibration profile of ^{14}C activity for the layered models (step function). The irregularly shaped shaded areas are traced from graphical presentations of Bien et al. (1965) of profiles taken at various locations in the Pacific and Indian Oceans, and the rectangles give ranges of samples from the indicated depth zones of the Atlantic Ocean reported by Broecker et al. (1960).

activity must agree as closely as the model's structure permits with that estimated for the real ocean. The mathematical structure of Model 3b imposes the first requirement, and the second would seem a desideratum for any model of carbon in the ocean. Application of these two constraints to the layered models, however, forces us to discard the observed depth information for the data points and to allow the depth distributions to be determined by eq. (3.5). Since the two-box models cannot approximate the real ocean's carbon-mass distribution of activity as closely as the layered models, we determine their distributions by requiring that $\sum_{j=1}^{N} A'_j y_j^0$ must be the same for them as for the layered models (i.e., the mean activities must agree) and $A'_1 = 0.96$. These requirements, in view of eq. (2.5), set the same mean transit time for all of the models.

The between-ocean variation of A' indicated by Fig. 4 raises the question of how the model ocean's dynamic characteristics would be affected by the inclusion of separate reservoirs calibrated to the distinct A' profiles of the Atlantic and Pacific (and possibly Indian) Oceans. An examination of this question is beyond the scope of the present report, but we expect to return to it in a subsequent paper.

4. Distributions of carbon transit time and age in the ocean models

In this section we state without proof the formulas used to compute carbon transit-time and age distributions for the five ocean models at steady state. Concepts and general results are discussed by Eriksson (1961), Bolin and Rodhe (1973), and Nir and Lewis (1975). See Zimmerman (1976) for a detailed example of a derivation of transit-time and age distributions and means from initial-value problems for a system of finite-difference equations corresponding to a box model.

If a unit mass of carbon is introduced into the surface-water compartment at time zero, we assume that the resultant excess amounts of carbon, η_i, $i = 1, \ldots, N$, satisfy the perturbation equations

$$\frac{d\eta_1}{dt} = -\left(\mu + \sum_{j=2}^{N} k_{1,j}\right)\eta_1 + \sum_{j=2}^{N} k_{j,1}\,\eta_j \tag{4.1}$$

$$\frac{d\eta_i}{dt} = -\left(\sum_{\substack{j=1 \\ j\neq i}}^{N} k_{i,j}\right)\eta_i + \sum_{\substack{j=1 \\ j\neq i}}^{N} k_{j,i}\,\eta_j, \quad i = 2, \ldots, N \tag{4.2}$$

where the transfer coefficients $k_{i,j}$ and evasion coefficient μ have been calculated from eqs. (2.3)–(2.5). The initial conditions for the system (4.1)–(4.2) are

$$\eta_i(0) = \begin{cases} 1 \text{ for } i = 1 \\ 0 \text{ for } 2 \le i \le N \end{cases} \tag{4.3}$$

representing the initial pulse of carbon in the surface-water compartment. Therefore, the fraction of the initial pulse remaining in the ocean at time t is

$$R(t) = \sum_{j=1}^{N} \eta_j(t), \qquad t \ge 0 \tag{4.4}$$

The distributions of transit time and age may be stated in terms of the function R, and thus their calculation from the solution of the system (4.1)–(4.3) is specified.

For transit time τ:

$$\Phi(\tau) = 1 - R(\tau) \tag{4.5}$$

where Φ is the normalized cumulative distribution function. Graphs of $\Phi(\tau)$ for the five models are shown in Fig. 5.

For age T:

$$\Psi(T) = \frac{\int_0^T R(t)\,dt}{\int_0^{+\infty} R(t)\,dt} \tag{4.6}$$

where Ψ is the normalized cumulative distribution function. Graphs of $\Psi(T)$ for the five ocean models are displayed in Fig. 6.

Elimination of R between eqs. (4.5) and (4.6) gives a general result proved by Bolin and Rodhe (1973).

The mean, $\bar{\tau}$, of the transit time of carbon entering the ocean at steady state is known to be

$$\bar{\tau} = M/I \tag{4.7}$$

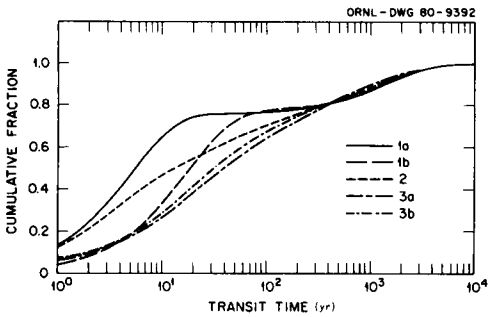

Fig. 5. Cumulative distribution of transit time of carbon entering the ocean from the atmosphere for each of the five ocean-reservoir models. The mean transit time is the same for all five: $\bar{\tau} = 393$ yr, while the median transit times range from 5.6 to 39 yr, indicating the dynamical differences among the models and the relative importance of the rapid-turnover carbon pools.

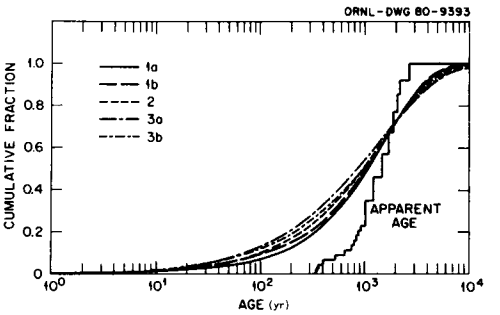

Fig. 6. Cumulative distributions of age of carbon in the steady-state ocean as represented by each of the five models. The step function represents "apparent age" distribution for the layered models (2, 3a, and 3b) and is constructed from ^{14}C activities of the layers. The discrepancy between this distribution and that of age for any of the models is due to the extent of mixing simulated by the model.

where I is the invasion rate and M is the total carbon mass in the ocean (Eriksson, 1961; Bolin and Rodhe, 1973; Nir and Lewis, 1975).

Let $\bar{T}$ denote the mean age of carbon in the ocean at steady state and $\bar{T}_i$ the mean age of carbon in compartment i (= 1, . . ., N). Then

$$\bar{T} = M^{-1} \sum_{i=1}^{N} y_i^0 \bar{T}_i \tag{4.8}$$

and the $\bar{T}_i$ may be calculated by solving the following linear algebraic system:

$$-\left(\mu + \sum_{j=2}^{N} k_{1,j}\right) y_1^0 \bar{T}_1 + \sum_{j=2}^{N} k_{j,1} y_j^0 \bar{T}_j = -y_1^0 \tag{4.9}$$

$$-\left(\sum_{\substack{j=1 \\ j \neq i}}^{N} k_{i,j}\right) y_i^0 \bar{T}_i + \sum_{\substack{j=1 \\ j \neq i}}^{N} k_{j,i} y_j^0 \bar{T}_j = -y_i^0, \qquad i =, \ldots, N \tag{4.10}$$

Table 3 shows the $\bar{T}_i$ and $\bar{T}$ for each of the five models. The "apparent age," given by $-\lambda^{-1} \ln A_i'$, is tabulated for comparison.

5. Integrated responses to atmospheric inputs

For the simulations described in this section, the time axis has been divided into two intervals as follows:

Interval 1: $1860 \leq t \leq 1975$
Interval 2: $1975 \leq t \leq 2300$

Each ocean model has been incorporated into a larger framework representing the world carbon cycle.

For integration over Interval 1, the historic release rate of fossil carbon and the atmospheric

Table 3. *Carbon age means (yr) for the five reservoir models*

Layer	Model 1a	1b	2	3a	3b	Apparent age*
1	393	393	393	393	393	337
2	1585	1585	401	403	403	346
3			419	422	422	363
4			454	462	462	398
5			578	601	601	520
6			706	741	740	644
7			809	852	850	743
8			857	903	900	789
9			905	955	950	834
10			944	997	990	871
11			983	1039	1031	908
12			1093	1152	1142	1010
13			1311	1380	1358	1208
14			1607	1677	1640	1471
15			1875	1940	1884	1701
16			2108	2167	2088	1896
17			2287	2345	2241	2043
18			2432	2503	2363	2160
19			3102	3102	2900	2681
Reservoir mean	1564	1514	1611	1663	1607	1450

* Apparent age $= -\lambda^{-1} \ln A_i'$ for layer i.

level of CO_2 are treated as known functions of time, as is the atmospheric ^{14}C activity from weapons testing. The purpose is to compare the five models with respect to their simulation of the ocean's uptake of CO_2 and weapons ^{14}C.

Integration over Interval 2 is different in the following respects: (1) Only nonradioactive carbon is simulated. (2) The atmospheric CO_2 level becomes one of the state variables rather than an exogenous function of time. It is driven by a fossil CO_2 release rate scenario to be described in this section. (3) Initial (t = 1975) conditions for all compartments were obtained from the companion integrations over Interval 1. (4) After 1975, net exchange of carbon with the terrestrial biosphere is assumed to be zero, except for a transitional period of a decade during which the exchange rate is varied from the initial value inherited from Interval 1 to zero.

The quantity of interest for Interval 2 is the resultant atmospheric level of CO_2 for each of the ocean models.

Interval 1:

The differential equations are

$$\frac{dY_1}{dt} = -\kappa_{m,a} P_m - \left(\sum_{j=2}^{N} k_{1,j}\right) Y_1 + \sum_{j=2}^{N} k_{j,1} Y_j + k_{a,m} Y_a \tag{5.1}$$

$$\frac{dX_1}{dt} = -\alpha_{m,a} \kappa_{m,a} P_m (X_1/Y_1) - \left(\sum_{j=2}^{N} k_{1,j} + \lambda\right) X_1 + \sum_{j=2}^{N} k_{j,1} X_j + \alpha_{a,m} k_{a,m} A_a^* Y_a \tag{5.2}$$

For $i = 2, \ldots, N$:

$$\frac{dY_i}{dt} = -\left(\sum_{\substack{j=1 \\ j\neq i}}^{N} k_{i,j}\right) Y_i + \sum_{\substack{j=1 \\ j\neq i}}^{N} k_{j,i} Y_j \tag{5.3}$$

$$\frac{dX_i}{dt} = -\left(\sum_{\substack{j=1 \\ j\neq i}}^{N} k_{i,j} + \lambda\right) X_i + \sum_{\substack{j=1 \\ j\neq i}}^{N} k_{j,i} X_j \tag{5.4}$$

where Y and X denote mass units of nonradioactive carbon (^{12}C + ^{13}C) and weapons ^{14}C, respectively, and λ is the decay constant for ^{14}C. The $k_{i,j}$ for the five models were derived as indicated in Section 2. The flux $\kappa_{m,a} P_m$ from the surface layer to the atmosphere is expressed in terms of the partial pressure, P_m, of dissolved CO_2 in the surface water, which is calculated from Y_1 at each integration step by a thermodynamic procedure (Keeling, 1973a; Bacastow and Keeling, 1973; Killough, 1980). With μY_1 equated to $\kappa_{m,a} P_m$, one may solve for a state-dependent coefficient $\mu = \mu(P_m)$ whose initial value is that of the linear-model coefficient derived previously ($\mu = \mu^0 =$ 0.148 yr^{-1} for Models 1a, 2, 3a, and 3b; and 0.0432 yr^{-1} for Model 1b); the indicated variation of μ (nonlinear in Y_1) expresses the shifting carbonate-bicarbonate chemistry of the surface water as carbon dioxide is added or removed. We denote atmospheric levels of nonradioactive carbon and ^{14}C by Y_a and $A_a^* Y_a$, respectively, where A_a^* denotes atmospheric ^{14}C activity due to weapons testing. Isotopic fractionation of ^{14}C with respect to ^{12}C in transfers between the atmosphere and surface waters is represented by the coefficients $\alpha_{a,m}$ and $\alpha_{m,a}$, estimated as 0.972 and 0.955, respectively (Keeling, 1973a).

Initial conditions for eqs. (5.1) and (5.3) are $Y_i(t_0) = y_i^0$, $i = 1, \ldots, N$, where the y_i^0 are grams of carbon assigned to the layers as shown in Table 1. For eqs. (5.2) and (5.4), the levels of weapons radiocarbon are set initially to zero.

The mass of airborne carbon, Y_a, is supplied to the model as an exogenous function of time:

$$Y_a = P_a \times 5.14 \times 10^{21} \times (12.011/28.964) \times 10^{-6}, \tag{5.5}$$

$$P_a = P_a^0 + d \cdot \exp[\alpha(t - 1958)], \tag{5.6}$$

where $P_a^0 = 290$, $d = 24.64$, and $\alpha = 12 \times 0.00247$ yr^{-1}. These units express the atmospheric CO_2 partial pressure, P_a, in parts per million by volume; 10^{-6} converts P_a to a mixing ratio, and the mass of the atmosphere (5.14×10^{21} g) and the ratio of gram-molecular weights of carbon and dry air (12.011/28.964) convert the mixing ratio to grams of airborne carbon. Equation (5.6) (Rust et al., 1979; Rust, private communication) is fitted to the atmospheric CO_2 data monitored at the Mauna Loa Observatory since 1958 by Keeling and his co-workers (Keeling et al., 1976).

Representation of the atmospheric ^{14}C from

detonations of nuclear weapons is based on data taken at several latitudes and summarized by Nydal et al. (1976). Our input function is an average of their time series for Nordkapp (71°06′ N, 23°59′ W) and Madagascar (21°27′ S, 47°05′ E), which we have interpolated linearly and sampled the interpolates at the interval 0.25 yr (Fig. 7).

Cumulative uptakes of nonradioactive carbon and ^{14}C are calculated from the integrations over Interval 1 as

$$\tilde{F}_{a,m}(t) = \int_{1860}^{t} [k_{a,m} Y_a(t') - \kappa_{m,a} P_m(t')]\, dt' \tag{5.7}$$

and

$$\tilde{F}^*_{a,m} = \int_{1945}^{t} \{\alpha_{a,m} k_{a,m} A^*_a(t') Y_a(t') - \alpha_{m,a} \kappa_{m,a} P_m(t') [X_1(t')/Y_1(t')]\}\, dt' \tag{5.8}$$

respectively; $\tilde{F}_{a,m}$ and $\tilde{F}^*_{a,m}$ are plotted vs time in Figs. 8 and 9, respectively.

A particularly interesting aspect of the historical integrations over Interval 1 is brought out by considering the response of a terrestrial biotic reservoir that would be required to close the system for each of the five ocean models. It is possible to calculate the cumulative *net* flux of nonradioactive carbon between the atmosphere and this reservoir as follows:

$$\tilde{F}_{a,b}(t) = -\int_{1860}^{t} \left[\frac{d}{dt'} Y_a(t') - f(t')\right] dt' - \tilde{F}_{a,m}(t), \tag{5.9}$$

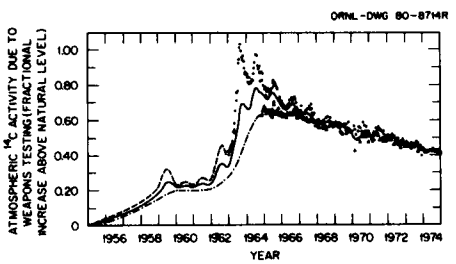

Fig. 7. Carbon-14 activity in the atmosphere due to weapons testing (fraction above natural level). Sample points: O Nordkapp (71°06′N, 23°59′E); △ Madagascar (21°27′S, 47°05′E); (Nydal et al., 1976). The solid curve is a cubic spline fitted to points interpolated between the levels at these stations. The curve was used for the simulations to compare uptake of bomb-produced ^{14}C by the five ocean-reservoir models.

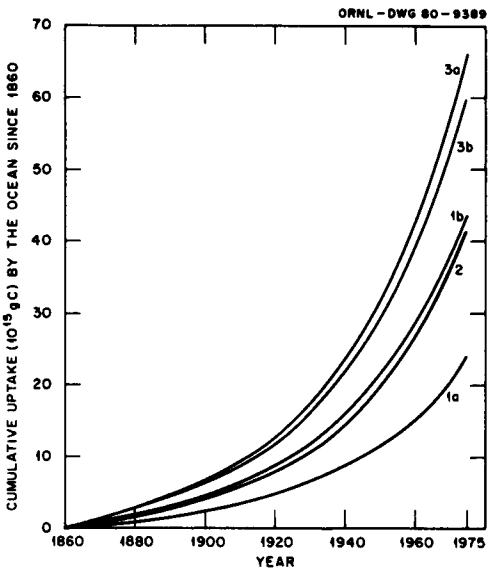

Fig. 8. Cumulative net uptake of the excess CO_2 by the five ocean-reservoir models for the period 1860–1975.

where $F_{a,m}(t)$ is the net uptake by the ocean to time t as given by equation (5.7); $f(t')$ is the historic rate of release of fossil CO_2 (units of 10^{15} gC yr^{-1}), which we have spline-interpolated from data of Keeling (1973b) and Rotty (1975) [see Killough (1980) for a table of the annual releases as compiled from these sources]. The time derivative, $dY_a(t')/dt'$, is computed from eqs. (5.5) and (5.6). Fig. 10 shows the graphs of (5.9) for the five models.

Interval-2 calculations are based on a logistic future release scenario for CO_2:

$$\frac{dp}{dt} = rp(1 - p/p_\infty), \qquad p(t_0) = p_0 \tag{5.10}$$

where $p(t)$ is the cumulative release of fossil carbon to time t and r is an initial rate parameter (= 0.043 for these simulations). The initial condition specifies the cumulative release of fossil carbon (= 134 × 10^{15} gC) from 1860 to the year t_0 = 1975. The parameter p_∞ represents the limiting release achieved as $t \to +\infty$; the value $p_\infty = 5000 \times 10^{15}$ gC was adopted as a reference value (Perry and Landsberg, 1977). The ocean surface temperature was held constant for these simulations, even though it would be expected to rise with increasing atmospheric CO_2, further reducing the ocean's capacity for uptake. But with the current range of

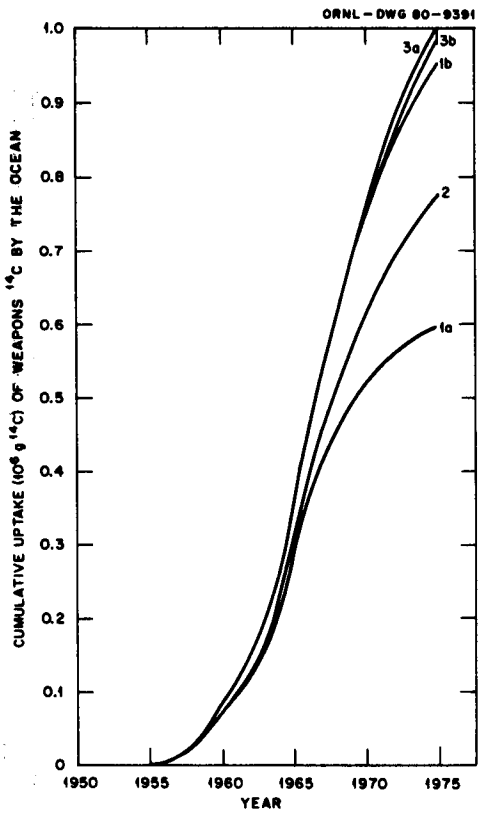

Fig. 9. Cumulative net uptake of ^{14}C from weapons tests by the five ocean-reservoir models for the period 1945–1975. Atmospheric levels were based on the solid curve of Fig. 7.

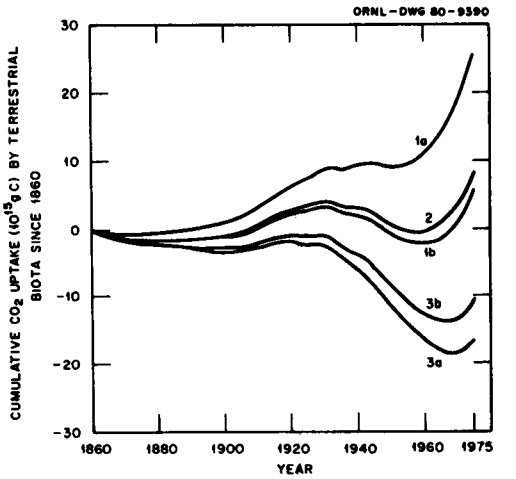

Fig. 10. Cumulative net uptake of excess CO_2 by terrestrial ecosystems for the period 1860–1975, estimated as the residual after the ocean's uptake is simulated by each of the five models, with atmospheric level given by an empirical fit to data [eq. (5.6)] and fossil fuel combustion history as estimated by Keeling (1973b) and Rotty (1975). The biota reservoir would be interpreted as a net sink for CO_2 in periods where the cumulative uptake curves have positive slope, such as in the years immediately preceding 1975. For possible confounding factors in the interpretation, see the text.

estimates ($\Delta T = 2.5 \rightarrow 3$ °C per doubling of CO_2; Manabe and Wetherald, 1975), our calculations and those of others (Bacastow and Keeling, 1979) show that the maximum effect on the simulated atmospheric CO_2 levels is a few percent. Fig. 11 shows the cumulative release and atmospheric response curves for the five models.

6. Discussion and conclusions

Our principal goal in performing the analyses reported here was to initiate a study of inherent structural differences in comparably calibrated mathematical models used to represent carbon dynamics in the ocean as those differences influence the larger system. In the present paper, we have limited our attention to one-dimensional models of the ocean.

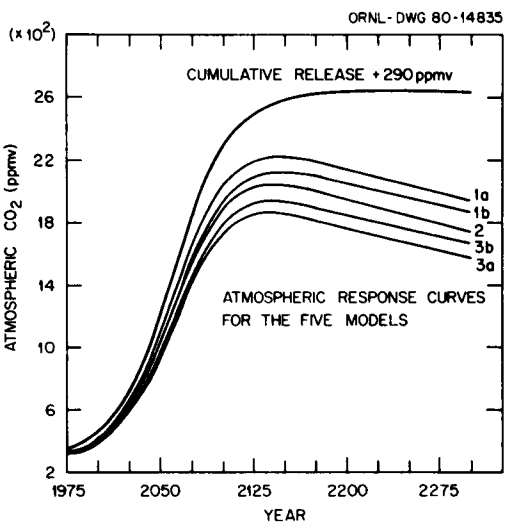

Fig. 11. Atmospheric response levels of CO_2 based on cumulative release as shown. Net exchange with terrestrial biota was assumed to be zero after an asymptotic transition period within the decade after 1975. The shifting CO_2-carbonate-bicarbonate balance is simulated for the ocean surface waters so that the evasion rate coefficient μ increases as a superlinear function of the surface waters' burden of excess CO_2.

A large part of the scientific debate concerning carbon-cycle dynamics has centered on the component of "excess" carbon that neither remains airborne nor is taken up by reservoir models of the ocean that have been proposed to date. Terrestrial-plant reservoirs have been added to the total cycle models to furnish a sink for this residual component, but this view of the land biota *qua* sink has been vigorously challenged (see Woodwell, 1978; Woodwell et al., 1978, and Broecker et al., 1979 for contrasting views of the terrestrial biota in the role of carbon sink). More elaborate representations of the ocean have been put forward, with response characteristics that have been reported to deal more successfully with the range of time constants in their forcing functions (historic fossil-fuel CO_2 production and ^{14}C from nuclear weapons tests) than their predecessors (Oeschger et al., 1975; Siegenthaler and Oeschger, 1978; Björkström, 1979). The "box-diffusion" model described by Oeschger et al. (1975), however, postulated a terrestrial reservoir which, within the context of the model's calibration, played the role of sink in the historic simulation (1860–1970), but Siegenthaler et al. (1978) experimented with scenarios of historic anthropogenic transfer of carbon from biota to atmosphere. The model discussed by Björkström (1979) appears to be designed to facilitate similar exercises.

The complexity of these and other models and the lack of a common calibration scheme tend to obscure the contribution of individual reservoirs resulting from the intrinsic dynamic properties of their mathematical representations. Therefore, comparisons among the models are very difficult. The kind of limited exercise that we have carried out with several ocean-reservoir prototypes is suggestive of procedures that might be undertaken in lieu of attempts to make direct comparisons of existing models.

Analysis of transit-time and age distributions of material moving through a model reservoir has long been advocated as fundamental to the interpretation of measurements of one or more tracers in a corresponding real system in order to discern its dynamic properties (Eriksson, 1961; Bolin and Rodhe, 1973; Nir and Lewis, 1975). Related "influence functions" also have been used to characterize and contrast reservoir models with respect to intrinsic dynamic properties (e.g., Welander, 1959; Eriksson, 1961, and their "frequency-response diagrams" in the complex plane). Such analyses provide valuable insight but need to be supplemented by investigations of reservoir behavior in the larger system when the object of investigation is the global carbon cycle. It is the combined examination of intrinsic reservoir properties and integrated responses to historic forcing functions, controlled by common calibration, that constitutes our point of view in the work reported here.

Fig. 5 shows the cumulative distribution curves for transit times of carbon entering the ocean at steady state—one curve for each of the five models. All five distributions have the same mean transit time: $\bar{\tau} = \sum y_i^0/I = 393$ yr [eqs. (4.7), (2.5), and Table 1]. Yet the distribution curves discriminate rather sharply among the models, with the exception that little difference is indicated between Models 3a and 3b, despite their structural difference. As an indication of extremes, we note that Model 1a returns 50% of the invading carbon to the atmosphere within 5.6 yr, while Model 3a requires 39 yr to return the same fraction. More generally, the curve for Model 3a lies below that of 1a for $\tau < \sim 400$ yr. Hence, at any time within that range, 3a will have returned a smaller fraction of an initial pulse than 1a. Thus, at the end of any given history of atmospheric carbon spanning no more than 400 yr, Model 3a will retain more of the invading carbon than 1a.

Model 1b, with its deeper surface layer (260 m), has its transit-time distribution curve in fair agreement with those of Models 3a and 3b for $1 \leq \tau \leq 8$ yr, but the separation becomes pronounced as τ increases. Since the curve for 1b lies above those for 3a and 3b over the longer period $10 < \tau < 400$ yr, one expects 1b generally to retain less carbon than 3a and 3b in simulations that extend at least over several decades. We shall see that this expectation is confirmed.

Comparison of the five distributions of transit time is of particular importance in the range $\tau < \sim 120$ yr for studying the history of the ocean's uptake of carbon in response to rising atmospheric levels. As Fig. 5 shows, the contrasts among the transit-time distribution curves are particularly pronounced over much of this range, raising the possibility of quite different simulated allocations of carbon among ocean, atmosphere, and terrestrial biota, according to which ocean model is chosen.

This possibility, as we shall show, is in fact realized.

The carbon age distributions shown in Fig. 6 offer little contrast among the models but differ markedly from the "apparent age" distribution (step function, Fig. 6) computed from the ^{14}C activity estimates A_i' of the layers: apparent age of carbon in layer $i = -\lambda^{-1} \ln A_i'$. The discrepancy between the apparent age distribution and those of the models is a measure of the mixing simulated by the latter, which reduces the variance of the activity distribution and distorts estimates of age (Nir, 1964; Eriksson, 1961). Thus, if any of the models represents a close approximation to the true age distribution, Fig. 6 demonstrates that direct estimation of age of water samples and flow rates by radiocarbon dating techniques is potentially inaccurate (cf. Kuo and Veronis, 1970).

Fig. 8 compares cumulative uptake of carbon by the five ocean models in response to a common history of atmospheric carbon in the period 1860–1975 [eqs. (5.5) and (5.6)]. Fig. 9 makes the analogous comparison for the weapons-produced ^{14}C (1955–1975; Fig. 7). Models 3a and 3b emerge by a significant margin as leaders in uptake capacity. For Model 3a, the cumulative net uptake of nonradioactive carbon is 66×10^{15} gC, while Model 1b leads Model 2 and Model 1a with a cumulative net uptake of 44×10^{15} gC. For radiocarbon, Models 3a, 1b, and 3b are closely clustered, with 1.0×10^6, 0.96×10^6, and 0.99×10^6 g of weapons ^{14}C, respectively, removed from the atmosphere. Both calculations place two-box Model 1a in last place with respect to carbon uptake: for nonradioactive carbon, 24×10^{15} vs 66×10^{15} gC, a factor of 2.8. In the light of the previous discussion of the cumulative distribution curves of transit time, the contrast in relative behavior of the models for nonradioactive carbon on the one hand and weapons ^{14}C on the other may be partially understood in terms of comparisons of the curves in Fig. 5 in relation to the different time scales of the source histories (115 vs 20 yr). The fundamentally different shapes of the forcing functions, $Y_a(t)$ and $X_a(t)$ (increasing vs decreasing exponential), accentuate the difference. The nonlinear dependence of the CO_2 partial pressure, P_m, on the carbon content, Y_1, of the surface waters may be expected to exert a lesser influence.

The residual carbon not taken up by the ocean models and not remaining airborne, which we formally attribute to the terrestial ecosystem reservoir, is plotted in Fig. 10, for each of the five models, as a cumulative net uptake curve. The extremes represented by these curves emphasize the potentially critical role of the terrestrial biota in complementing calculation. Whereas many previous modeling approaches have prescribed deterministic mechanisms for the compartments associated with the terrestrial biota (often assuming *a priori* that the reservoir must act as a sink for the excess CO_2), no such assumptions have been made in this calculation. It is essential to remember, however, that each of the curves of Fig. 10, which we are interpreting as cumulative net biotic uptake, also contains a residual error composed of the effects of (1) the model ocean's deviation from the real ocean's historic exchange of carbon with the atmosphere, (2) the departure of eqs. (5.5) and (5.6) from the true record of total CO_2 in the atmosphere, and (3) errors of estimation of past and present releases of fossil CO_2. Moreover, the atmospheric CO_2 history [eq. (5.6)] is based entirely on a least-squares fit of an exponential curve to data taken at the Mauna Loa Observatory during the period 1958–1975, subject to the assumption of a primordial level of 290 ppmv. Therefore, the relationship between this curve and the annual fossil CO_2 production data before 1958 could differ significantly from the true (but essentially unknown) record.

Two other aspects of the biotic uptake curves of Fig. 10 should be noted. First is the range: Model 1a predicts a gain of 26×10^{15} gC between 1860 and 1975 vs a loss of 17×10^{15} gC estimated by Model 3a. Second is the return of each curve to a positive slope in the years preceding 1975. The interpretation of the latter phenomenon, if real, is the shift of role of the biotic reservoir from that of a net source for atmospheric CO_2 to that of a sink. The maximum predicted net uptake rate for the beginning of the year 1975 is 1.6×10^{15} gC yr^{-1} (Model 1a) vs 0.39×10^{15} gC yr^{-1} (Model 3a) for the minimum. It remains to be demonstrated more directly whether the upturn in the cumulative uptake curves of Fig. 10 represents a real shift of role in the participation of the biotic reservoir in carbon-cycle dynamics. The loss of carbon biomass estimated by Model 3a is gradual, at an average rate of $(17 \times 10^{15}$ gC)/(115 yr) $= 0.15 \times 10^{15}$ gC yr^{-1}, with a maximum loss rate of 0.74×10^{15} gC yr^{-1} at the beginning

of the year 1946. Such loss rates are moderate by comparison with some estimates. For example, $(4 \rightarrow 8) \times 10^{15}$ gC yr^{-1} was the estimate presented by G. M. Woodwell to the U.S. Senate Committee on Governmental Affairs July 30, 1979 (U.S. Senate, 1979). Also see Woodwell (1978) and Woodwell et al. (1978). Estimates of $\sim(1 \rightarrow 2) \times 10^{15}$ gC yr^{-1} have been presented by Bolin (1977), Stuiver (1978), and Chan et al. (1979).

Fig. 11 compares the atmospheric response CO_2 levels for the future scenario of release that is shown there as a cumulative plot [eq. (5.10) with $p_\infty = 5000 \times 10^{15}$ gC]. The maximum ordinates on the response curves of Models 1a and 3a differ by about 350 ppmv, roughly the quantity of CO_2 in the atmosphere at present. We caution that Fig. 11 is offered only as a comparison of the models' responses over a long integration period that includes steeply rising and ultimately declining source-function behavior. We cannot enter here into the question of its validity as a forecast of fossil CO_2 release or consequent atmospheric levels.

The analysis of ocean models for carbon turnover with different one-dimensional structures for representing the circulation of carbon in the ocean as presented here is not meant to identify a single structure or parameter set as best in the sense of passing various tests of conformity of predictions with observations (Broecker et al., 1979). Models that separate the Atlantic and Pacific Oceans or that consider variation with latitude have not yet been included in our comparison, nor have we discussed sensitivity of the predictions to variations in parameters. We expect to deal with these matters in subsequent papers.

At the present stage of our experience, we believe that empirically calibrated box models offer a flexible and powerful tool for exploring a variety of hypotheses relating to carbon-cycle dynamics. Ultimately we expect that general-circulation-type models that incorporate detailed patterns of water transport, air-sea gas exchange, and improved quantification of dynamic chemical and biological processes will become the research tools of choice.

7. Acknowledgements

A number of our colleagues have given us advice and assistance in connection with this work and its exposition. We are very grateful to R. Nydal, Laboratoriet for Radiologisk Datering, Trondheim, Norway, for providing tabular data corresponding to his measurements of atmospheric $\Delta^{14}C$ which he and his coworkers have meticulously assembled over the years and published in graphical form. We also wish to acknowledge several helpful discussions during early stages of this work with A. Nir, Isotope Department, Weizmann Institute of Science, Rehovot, Israel. For critical technical reviews of this manuscript and related material, we are indebted to R. V. O'Neill and D. L. DeAngelis, Environmental Sciences Division, Oak Ridge National Laboratory (ORNL) and C. C. Travis and D. E. Fields, Health and Safety Research Division, ORNL. Linda Allison, Information Division, ORNL, has our heartfelt thanks for her capable, cheerful, and indispensable information services.

Finally, we wish to thank two of our colleagues for many ideas and discussions over a period of years: J. S. Olson, Environmental Sciences Division, ORNL, and R. J. Mulholland, Oklahoma State University, Stillwater, Oklahoma.

This research was supported jointly by the National Science Foundation's Ecosystem Studies Program under Interagency Agreement No. DEB 77-26722 and the Carbon Dioxide Effects Research and Assessment Program, U.S. Department of Energy, under contract W-7405-eng-26 with Union Carbide Corporation.

REFERENCES

Bacastow, R. and Keeling, C. D. 1973. Atmospheric carbon dioxide and radiocarbon in the natural carbon cycle: II. Changes from A.D. 1700 to 2070 as deduced from a geochemical model. In *Carbon and the biosphere* (eds. G. M. Woodwell and E. V. Pecan). CONF-720510. Springfield Va.: National Technical Information Service, 86-135.

Bacastow, R. and Keeling, C. D. 1979. Models to predict future atmospheric CO_2 concentrations. In *Global effects of carbon dioxide from fossil fuels* (eds. W. P. Elliott and L. Machta). CONF-770385. Springfield Va.: National Technical Information Service, 72–90.

Bien, G. and Suess, H. 1967. Transfer and exchange

of ^{14}C between the atmosphere and the surface water of the Pacific Ocean. In *Radioactive dating and methods of low-level counting*. Vienna: International Atomic Energy Agency, 105–115.

Bien, G. S., Rakestraw, N. W. and Suess, H. 1965. Radiocarbon in the Pacific and Indian Oceans and its relation to deep water movements. *Limnol. Oceanogr. 10* (Suppl.), R25–R37.

Björkström, A. 1979. A model of CO_2 interaction between atmosphere, oceans, and land biota. In *The global carbon cycle—SCOPE 13* (eds. B. Bolin, E. T. Degens, S. Kempe and P. Ketner). New York: Wiley, 403–451.

Bolin, B. 1975. A critical appraisal of models for the carbon cycle. In *Global atmospheric research program, the physical basis of climate and climate modeling, Pub. 16*. New York: World Meteorological Organization—International Council of Scientific Unions, 225–235.

Bolin, B. 1977. Changes of land biota and their importance for the carbon cycle. *Science 196*, 613–615.

Bolin, B. and Rodhe, H. 1973. A note on the concepts of age distribution and transit time in natural reservoirs. *Tellus 25*, 58–62.

Broecker, W. S. 1963. Radioisotopes and large-scale oceanic mixing. In *The sea*, Vol. 2 (ed. M. N. Hill). New York: Wiley-Interscience, 88–108.

Broecker, W. S. 1974. *Chemical oceanography*. New York: Harcourt Brace Jovanovich.

Broecker, W. S. and Olson, E. A. 1959. Lamont radiocarbon measurements, 6. *Am. J. Sci., Radiocarbon Suppl. 1*, 111–132.

Broecker, W. S., Gerard, R., Ewing, M. and Heezen, B. C. 1960. Natural radiocarbon in the Atlantic Ocean. *J. Geophys. Res. 65*, 2903–2931.

Broecker, W. S., Peng, T.-H. and Stuiver, M. 1978. An estimate of the upwelling rate in the equatorial Atlantic based on the distribution of bomb radiocarbon. *J. Geophys. Res. 83*, 6179–6186.

Broecker, W. S., Takahashi, T., Simpson, H. J. and Peng, T.-H. 1979. Fate of fossil fuel carbon dioxide and the global carbon budget. *Science 206*, 409–417.

Craig, H. 1957. The natural distribution of radiocarbon and the exchange time of carbon dioxide between atmosphere and sea. *Tellus 9*, 1–17.

Chan, Y.-H., Olson, J. S. and Emanuel, W. R. 1979. *Simulation of land-use patterns affecting the global carbon cycle*, ORNL/TM-6551. Oak Ridge, Tenn.: Oak Ridge National Laboratory.

Eriksson, E. 1961. Natural reservoirs and their characteristics. *Geofísica Internacional 1*, 27–43.

Fairhall, A. W., Young, A. W. and Bradford, P. A. 1972. Radiocarbon in the sea. In *Proc. 8th int. conf. on radiocarbon dating, Wellington, New Zealand, October 1972*, C2–C16.

Keeling, C. D. 1973a. The carbon dioxide cycle: reservoir models to depict the exchange of atmospheric carbon dioxide with the oceans and land plants. In *Chemistry of the lower atmosphere* (ed. S. I. Rasool). New York: Plenum Press, 251–328.

Keeling, C. D. 1973b. Industrial production of carbon dioxide from fossil fuels and limestone. *Tellus 25*, 174–198.

Keeling, C. D. and Bacastow, R. 1977. Impact of industrial gases on climate. In *Energy and climate*, Geophysics Study Committee, Geophysics Research Board, Assembly of Mathematical and Physical Sciences, Washington, D.C.: National Academy of Sciences, 72–95.

Keeling, C. D., Bacastow, R. B., Bainbridge, A. E., Ekdahl, C. A., Guenther, P. R., Waterman, L. S. and Chin, J. F. S. 1976. Atmospheric carbon dioxide variations at Mauna Loa Observatory, Hawaii. *Tellus 28*, 538–551.

Killough, G. G. 1980. A dynamic model for estimating radiation dose to the world population from releases of ^{14}C to the atmosphere. *Health Phys. 38*, 269–300.

Kuo, H. H. and Veronis, G. 1970. Distribution of tracers in the deep oceans of the world. *Deep-Sea Res. 17*, 29–46.

Kuo, H. H. and Veronis, G. 1973. The use of oxygen as a test for an abyssal circulation model. *Deep-Sea Res. 20*, 871–888.

Lewis, S. and Nir, A. 1978. On tracer theory in geophysical systems in the steady and non-steady state. Part II. Non-steady state—theoretical introduction. *Tellus 30*, 260–271.

Manabe, S. and Wetherald, R. T. 1975. The effects of doubling the carbon dioxide concentration on the climate of a general circulation model. *J. Atmos. Sci. 32*, 3–15.

Nir, A. 1964. On the interpretation of tritium 'age' measurements of groundwater. *J. Geophys. Res. 69*, 2589–2595.

Nir, A. and Lewis, S. 1975. On tracer theory in geophysical systems in the steady and non-steady state. Part I. *Tellus 27*, 372–383.

Nydal, R., Lövseth, K. and Gulliksen, S. 1976. A survey of radiocarbon variation in nature since the Test Ban Treaty. *Proc. 9th Int. Radiocarbon Conf., U. of California at Los Angeles and San Diego* (in press).

Oeschger, H., Siegenthaler, U., Schotterer, U. and Gugelmann, A. 1975. A box diffusion model to study the carbon dioxide exchange in nature. *Tellus 27*, 168–192.

Östlund, H. G. and Stuiver, M. 1980. GEOSECS Pacific radiocarbon. *Radiocarbon 22*, 25–53.

Perry, H. and Landsberg, H. H. 1977. Projected world energy consumption. In *Energy and climate*, Geophysics Study Committee, Geophysics Research Board, Assembly of Mathematical and Physical Sciences, Washington, D.C.: National Academy of Sciences, 35–50.

Revelle, R. and Suess, H. E. 1957. Carbon dioxide exchange between atmosphere and ocean and the questions of an increase of atmospheric CO_2 during the past decades. *Tellus 9*, 18–27.

Rotty, R. M. 1975. *A note updating carbon dioxide production from fossil fuels and cement*, IEA (M)-75-4. Oak Ridge, Tenn.: Oak Ridge Associated Universities—Institute for Energy Analysis.

Rust, B. W. 1979. Private communication.

Rust, B. W., Rotty, R. M. and Marland, G. 1979. Inferences drawn from atmospheric CO_2 data. *J. Geophys. Res. 84*, 3115–3122.

Siegenthaler, U. and Oeschger, H. 1978. Predicting future atmospheric carbon dioxide levels. *Science 199*, 388–395.

Stuiver, M. 1978. Atmospheric carbon dioxide and carbon reservoir changes. *Science 199*, 253–258.

Stuiver, M. and Östlund, H. G. 1980. GEOSECS Atlantic radiocarbon. *Radiocarbon 22*, 1–24.

Sverdrup, H. U., Johnson, M. W. and Fleming, R. H. 1942. *The oceans—their physics, chemistry, and general biology*. New York: Prentice-Hall, Inc.

United States Senate. 1979. *Carbon dioxide accumulation in the atmosphere, synthetic fuels, and energy policy—a symposium*. Washington, D.C.: U.S. Government Printing Office.

Welander, P. 1959. On the frequency response of some different models describing the transient exchange of matter between the atmosphere and the sea. *Tellus 11*, 348–354.

Woodwell, G. M. 1978. The carbon dioxide question. *Sci. Am. 238*, 34–43.

Woodwell, G. M., Whittaker, R. H., Reiners, W. A., Likens, G. E., Delwiche, C. C. and Botkin, D. B. 1978. The biota and the world carbon budget. *Science 199*, 141–146.

Zimmerman, J. T. F. 1976. Mixing and flushing of tidal embayments in the western Dutch Wadden Sea. Part I: Distribution of salinity and calculation of mixing time scales. *Netherlands J. of Sea Res. 10*, 149–191.

СРАВНЕНИЕ НЕКОТОРЫХ МОДЕЛЕЙ ПЕРЕНОСА УГЛЕРОДА В ОКЕАНЕ В ОТНОШЕНИИ ИХ РАСПРЕДЕЛЕНИЙ ВРЕМЕНИ ПЕРЕНОСА И ВОЗРАСТА И ИХ РЕАКЦИИ К АТМОСФЕРНЫМ CO_2 И ^{14}C

Сравниваются пять моделей распределения углерода по глубине в мировом океане в отношении распределения времени переноса углерода, распределения по возрасту и реакции к CO_2 от ископаемых топлив и ^{14}C от атомных взрывов. Две модели представляют океан как два хорошо перемешанных слоя и отличаются друг от друга лишь относительными объемами этих частей. Остающиеся три модели рассматривают 19 хорошо смешанных слоев и отличаются типами переноса между этими слоями. Все 5 моделей должны быть совместимыми с профилем природного ^{14}C допромышленной эры, который используется для определения величин коэффициентов переноса. В рамках этого требования эти 5 моделей дают реакции, значительно отличающиеся друг от друга, на CO_2 от ископаемых топлив и ^{14}C от взрывов. Из оцениваемых 134×10^{15} г ископаемого углерода, произведенных в 1860–1975 гг., модели дают оценки чистого поглощения углерода океаном в диапазоне 24×10^{15}–66×10^{15} г C (углерода). Для ^{14}C от взрывов диапазон колеблется в пределах 6×10^{2}–1×10^{3} кг ^{14}C. Каждая из этих моделей показывает изменения в предполагаемой роли наземной биоты—от источника до стока углерода, причем последняя роль преобладает в последние годы периода моделирования. По самой высокой оценке в моделях величина источника углерода была равна 0.74×10^{15} г C в год, что следует сопоставить с производством CO_2 от ископаемых топлив 5×10^{15} г C в год в 1975 г. Эти пять моделей использовались также для предсказаний уровней атмосферного CO_2 в течение 1975–2300 гг. для некоторого источника, который в конечном итоге выпустит 5000×10^{15} г C.